Research Article Open Access

Shivaji G.Chavan* and Achchhe Lal

Bending analysis of laminated SWCNT Reinforced functionally graded plate Using FEM

DOI 10.1515/cls-2017-0010
Received Nov 09, 2016; accepted Jan 20, 2017

Abstract: In this paper presents bending characteristic of multi-layered carbon nanotube reinforced functionally graded composite plates. The finite element implementation of bending analysis of laminated composite plate via well-established higher order shear deformation theory (HSDT). A seven degree of freedom and C_0 continuity finite element model using nine noded isoperimetric elements is developed for precise computation of ply-by-ply deflection and stresses of laminated Single Wall Carbon Nanotube Reinforced composite plate subjected to uniform transverse loading. The finite element implementation is carried out through a finite element code developed in MATLAB. The results obtained by present approach are compared with results available in the literatures. The effective material properties of the laminated SWCNTRC plate are used by Mori-Tanaka method. Numerical results have been obtained with different parameters, width-to-thickness ratio (a/h), stress distribution profile along thickness direction, different SWCNTRC-FG plate, boundary condition and various lamination schemes.

Keywords: Micromechanical Analysis; HSDT Formulation; Finite Element Method for SWCNTR Laminated Plate; Numerical Analysis

1 Introduction

Single walled carbon nanotube (SWCNTs) is outstanding physical and chemical properties such as a high strength, high stiffness, high corrosion resistance and low density. Widely used in the subject area of aerospace, missile, automobile and civil construction etc. In advance many researchers have concentrated on the mechanical behavior of SWCNT reinforced composite beam, plate and shell. S. Jedari Salami [1] demonstrated Extended high order sandwich panel theory for bending analysis of sandwich beams with carbon nanotube reinforced face sheets. J. Wuite *et al.* [2] presented deflection and stresses behaviour of a carbon nanotube composite plate. Vodenitcharova *et al.* [3] presented the bending analysis of laminated composite plate. The buckling analysis of quadrilateral laminated thin-to-moderate and thick plate with carbon nanotube reinforced composite layer were demonstrated by P. Malekzadel *et al.* [4]. Wattanaskulong *et al.* [5] focused mead on single walled carbon nanotube configuration of distributed structure spread throughout the length of the plate with some thickness as UD, FG-O, FG-V, FG-X and FG-A. Lei *et al.* [6] presented large deflection analysis of functionally graded (FG) reinforced composite plate using the KP Ritz method. They used first order shear deformation plate theory (FSDT) and geometric nonlinearity on the basis of von Karman strain formulation. Lei *et al.* [7] developed a multi scale analysis of the bending and stress behaviour of the carbon nanotube beam. Zhu *et al.* [8] investigated bending and free vibration characteristic of SWCNTRC plate using Finite Element Method (FEM), which is based on FSDT. Madhu *et al.* [9] examined deflection and stresses on the SWCNTR composite plate using CLPT, FSDT and HSDT. They also studied effect of a/h, z/h and volume fraction of the CNT on a plate. The stress-strain behaviour and elastic properties of the carbon nanotube composite beam using Representative Volume Element (RVE) method were reported by Mohammadpour *et al.* [10]. Seidel *et al.* [11] and Hu.*et al.* [12] presented elastic property of SWCNTRC evaluated by using micromechanics model Mori-Tanaka. Dong-Li-Shi *et al.* [13] explained self-consistent model for In-plane elastic properties of grapheme SWCNT composite material. Stress analysis of thick laminated plate subjected to trigonometry shear deformation theory was presented by Ghugal *et al.* [14]. Sayyad *et al.* [15] investigated the behaviour of the

***Corresponding Author: Shivaji G.Chavan:** Research Scholar, Department of Mechanical Engineering, S.V. National Institute of Technology, Surat - 395007, India; shivajigchavan@gmail.com; Tel.: +91 9512534802
Achchhe Lal: Assistant Professor, Department of Mechanical Engineering, S.V. National Institute of Technology, Surat - 395007, India

out - plane and in-plane stress observed due to the effects of stress concentration.

Soraya Mareishi *et al.* [16] presented an analytical solution for nonlinear free and forced vibration response of smart laminated nano-composite beams resting on a nonlinear elastic foundation and under external harmonic excitation. They also studied Different distribution patterns of the single walled aligned and straight carbon nanotubes (SWCNTs) through the thickness of the beam. Kundalwal *et al.* [17] investigated the effect of carbon nanotube (CNT) waviness on the active constrained layer damping (ACLD) of the laminated hybrid composite shell. Pouresmaeeli *et al.* [18] reported vibration characteristics of moderately thick doubly curved functionally graded composite panels reinforced by carbon nanotube. Guz *et al.* [19] reviewed structurally complex Nano composites; their fillers have a complex shape, which complicates the theoretical analysis of these composites. Pantano *et al.* [20] analyzed numerical model for composite material with polymer matrix reinforced with carbon nanotubes. Wan *et al.* [21] presented a structural mechanics approach for predicting the mechanical properties of carbon nanotubes. Cestari *et al.* [22] studied an experimental research activity on the application of a polymeric resin reinforced with carbon nanotubes on an ancient timber structure belonging to cultural heritage. Kiani [23] investigated free vibrations of elastically embedded stocky single-walled carbon nanotubes acted upon by a longitudinally varying magnetic field. Mirzaei *et al.* [24] reported thermally induced bifurcation buckling of rectangular composite plates reinforced with single walled carbon nanotubes. Canadija *et al.* [25] investigated elastic properties of Nano-composite materials influence of carbon nanotube imperfections and interface bonding. Kamarian *et al.* [26] presented Eshelby-Mori-Tanaka approach for the vibrational behavior of functionally graded carbon nanotube-reinforced plate resting on elastic foundation. Shams *et al.* [27] studied buckling of laminated carbon nanotube-reinforced composite plates on elastic foundations using a mesh-free method.

However, in the literature, there are few studies about numerical analysis of laminated SWCNTR-FG plates. Therefore, in the present work Bending analysis of laminated SWCNT Reinforced functionally graded plate Using FEM, which is embedded of perfectly bonded SWCNTR-FG layers. In each SWCNT layer of plate, SWCNT is assumed to uniformly distribute in the thickness direction. Effective materials properties of the Nano-composites are calculated through Mori-Tanaka model. The higher order shear deformation theory is employed to determine for shear deformation. The investigate influence plate width to thickness ratio, distribution of SWCNT and stress distribution along plate thickness direction and lamination scheme on the bending response of laminated functionally graded plates.

2 Micromechanics Analysis

The effective material prosperity is evaluated by using Mori-Tanaka. This is a well-known model which is widely used in SWCNT composite plate. The carbon nanotube composite plate is made up of matrix Epon 862 and SWCNT. The stress and strain constitute equation is expressed as

$$\begin{bmatrix}\sigma_{11}\\ \sigma_{22}\\ \sigma_{33}\\ \sigma_{23}\\ \sigma_{13}\\ \sigma_{12}\end{bmatrix} = \begin{bmatrix} n & l & l & 0 & 0 & 0\\ l & k+m & k-m & 0 & 0 & 0\\ l & k-m & k+m & 0 & 0 & 0\\ 0 & 0 & 0 & 2m & 0 & 0\\ 0 & 0 & 0 & 0 & 2p & 0\\ 0 & 0 & 0 & 0 & 0 & 2p\end{bmatrix}\begin{bmatrix}\varepsilon_{11}\\ \varepsilon_{22}\\ \varepsilon_{33}\\ \varepsilon_{23}\\ \varepsilon_{13}\\ \varepsilon_{12}\end{bmatrix} \quad (1)$$

$$\boldsymbol{C} = \begin{bmatrix} n & l & l & 0 & 0 & 0\\ l & k+m & k-m & 0 & 0 & 0\\ l & k-m & k+m & 0 & 0 & 0\\ 0 & 0 & 0 & 2m & 0 & 0\\ 0 & 0 & 0 & 0 & 2p & 0\\ 0 & 0 & 0 & 0 & 0 & 2p\end{bmatrix} \quad (2)$$

Where, k, l, m, n and m are hill elastic constant's is uniaxial tension modulus in the fiber direction; k is plane-strain bulk modulus normal to the fiber direction. l is associated cross modulus, m and p is the shear modulus in planes normal and parallel to fibre direction represented by [9]. The Mori-Tanaka Method by [11], in the research problem, consider of its simplicity and accuracy at a high volume fraction of SWCNT as inclusion. The tensor of the effective elastic modulus **C** of SWCNT composite reinforced by aligning inclusion of the same can be defined by [13]

$$C = (V_m H_m + V_{CNT} H_{CNT} : A) : (V_m I + V_{CNT} A)^{-1} \quad (3)$$

H_m and $H_{CNT}$is tensor of elastic modulus of the corresponding phases. $I$is forth order identity tensor, A is fourth order average stress or strain expressed as

$$A = \left[\mathrm{I} + \mathrm{S} : {H_m}^{-1} : (H_{CNT} - H_m)\right]^{-1} \quad (4)$$

Where, S is Eshelby tensor for straight long SWCNT,

$$S_{1111} = S_{3333} = \frac{5 - 4\nu_m}{8(1-\nu_m)}, \quad (5)$$

$$S_{1122} = S_{3322} = \frac{v_m}{2(1-v_m)},$$
$$S_{1133} = S_{3311} = \frac{4v_m - 1}{8(1-v_m)} \quad S_{2323} = S_{1212} = \frac{1}{4};$$
$$S_{1313} = \frac{3-4v_m}{8(1-v_m)}$$

A-Tensor as

$$A_{1111} = A_{3333} = -\frac{C_3}{C_1C_2}, \quad A_{1133} = A_{3311} = \frac{C_4}{C_1C_2} \tag{6}$$
$$A_{1122} = A_{3322} = \frac{l_{CNT}(1-v_m-2v_m{}^2) - E_m v_m}{C_1}; \quad A_{2222} = 1;$$
$$A_{2323} = A_{1212} = \frac{E_m}{E_m + 2p_{CNT}(1+v_m)};$$
$$A_{1313} = \frac{2E_m(1+v_m)}{C_2}$$

Here,

$$C_1 = (-1+2v_m)[E_m + 2k_{CNT}(1+v_m)] \tag{7}$$
$$C_2 = E_m + 2m_{CNT}(3 - v_m - 4v_m{}^2);$$
$$C_3 = E_m(1-v_m)\left\{E_m(3-4v_m) + 2(1+v_m)\left[m_{CNT}(3-4v_m) + k_{CNT}(2-4v_m)\right]\right\}$$
$$C_4 = E_m(1-v_m)\left\{E_m(1-4v_m) + 2(1+v_m)\left[m_{CNT}(3-4v_m) + k_{CNT}(2-4v_m)\right]\right\}$$

The hill elastic constant is defined as,

$$k_{CNT} = \frac{E_{22}^{CNT}}{2(1 - v_{23}^{CNT} - 2v_{12}^{CNT}v_{21}^{CNT})}; \tag{8}$$
$$l_{CNT} = \frac{v_{21}^{CNT}E_{11}^{CNT}}{(1 - v_{23}^{CNT} - 2v_{12}^{CNT}v_{21}^{CNT})} = \frac{v_{12}^{CNT}E_{22}^{CNT}}{(1 - v_{23}^{CNT} - 2v_{12}^{CNT}v_{21}^{CNT})};$$
$$n_{CNT} = \frac{(1-v_{23}^{CNT})E_{11}^{CNT}}{(1 - v_{23}^{CNT} - 2v_{12}^{CNT}v_{21}^{CNT})}, \quad p_{CNT} = G_{12^{CNT}_{12}}, \quad m_{CNT} = G_{23}^{CNT}$$

The hill elastic constant is substitute Eq. (8) into Eq. (7) and calculate A-Tensor. Now Eq. (6), Eq. (5) and Eq. (4) are substitute in Eq. (3) for calculate C matrix. Compare Eq. (3) and Eq. (2) will get exact values of Hills elastic moduli.

$$k = \frac{E_m\{E_mV_m + 2k_{CNT}(1+v_m)[1+V_{CNT}(1-2v_m)]\}}{2(1+v_m)[E_m(1+V_{CNT}-2v_m) + 2V_mk_{CNT}(1-v_m-2v_m^2)]} \tag{9}$$
$$l = \frac{E_m\left\{V_mv_m[E_m + 2k_{CNT}(1+v_m)] + 2V_{CNT}l_{CNT}(1-v_m^2)\right\}}{(1+v_m)[E_m(1+V_{CNT}-2v_m) + 2V_mk_{CNT}(1-v_m-2v_m^2)]}$$
$$n = \frac{E_m^2V_m(1+V_{CNT}-V_mv_m) + 2V_mv_{CNT}(k_{CNT}n_{CNT} - l_{CNT}^2)(1-2v_m)}{(1+v_m)[E_m(1+V_{CNT}-2v_m) + 2V_mk_{CNT}(1-v_m-2v_m^2)]} + \frac{E_m[2V_m^2k_{CNT}(1-v_m) + V_{CNT}n_{CNT}(1-2v_m+V_{CNT}) - 42V_ml_{CNT}v_m]}{2V_mk_{CNT}(1-v_m+v_m^2) + E_m(1-V_{CNT}+2v_m)}$$
$$p = \frac{E_m[E_mV_m + 2(1+V_{CNT})p_{CNT}(1+v_m)]}{2(1+v_m)[E_m(1+V_{CNT}) + 2V_mp_{CNT}(1+v_m)]}$$
$$m = \frac{E_m[E_mV_m + 2m_{CNT}(1+v_m)(3+V_{CNT}-4v_m)}{2(1+v_m)\{E_m[(V_m + 4V_{CNT}(1-v_m)] + 2V_mm_{CNT}(3-v_m-4v_m^2)]\}}$$

The Fig. 1 shows Single walled carbon nanotubes are aligned and straight-line arrangement of composite plate, the elastic modulus of SWCNTRC plat is defined by

$$E_{11} = n - \frac{l^2}{k}; \quad E_{22} = \frac{4m(kn-l^2)}{kn - l^2 + mn}; \tag{10}$$
$$G_{12} = G_{13} = 2p; v_{12} = \frac{l}{2k} \quad v_{21} = \frac{v_{12}E_{22}}{E_{11}}$$

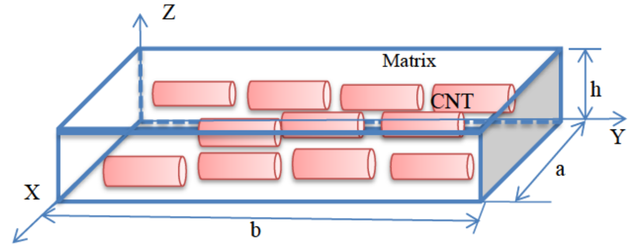

Figure 1: Straight aligned SWCNT, single layered SWCNTRC plate

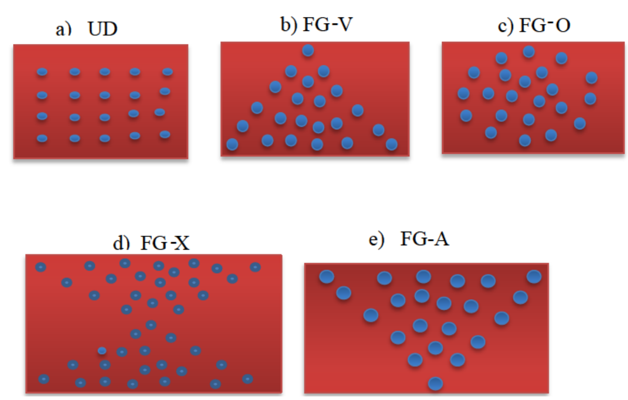

Figure 2: Different configuration of SWCNT-FG layers: a)UD, b) FG-A, c)FG-O, d) FG-X and e) FG-V

In this study consider the laminated SWCNTRC-FG plate with five configurations of SWCNTRC plates over the thickness as shown in Fig. 2. The mathematically modelled can be expressed by [6, 29],

$$V_{CNT} = V^* \text{---------------UD} \tag{11}$$
$$V_{CNT} = 2\left(1 - \frac{2|z|}{h}\right) V^* \text{--------FG-O}$$
$$V_{CNT} = \left(\frac{2|z|+h}{h}+\right) V^* \text{------- FG-V}$$
$$V_{CNT} = 4\left(\frac{|z|}{h}+\right) V^* \text{----------- FG-X}$$

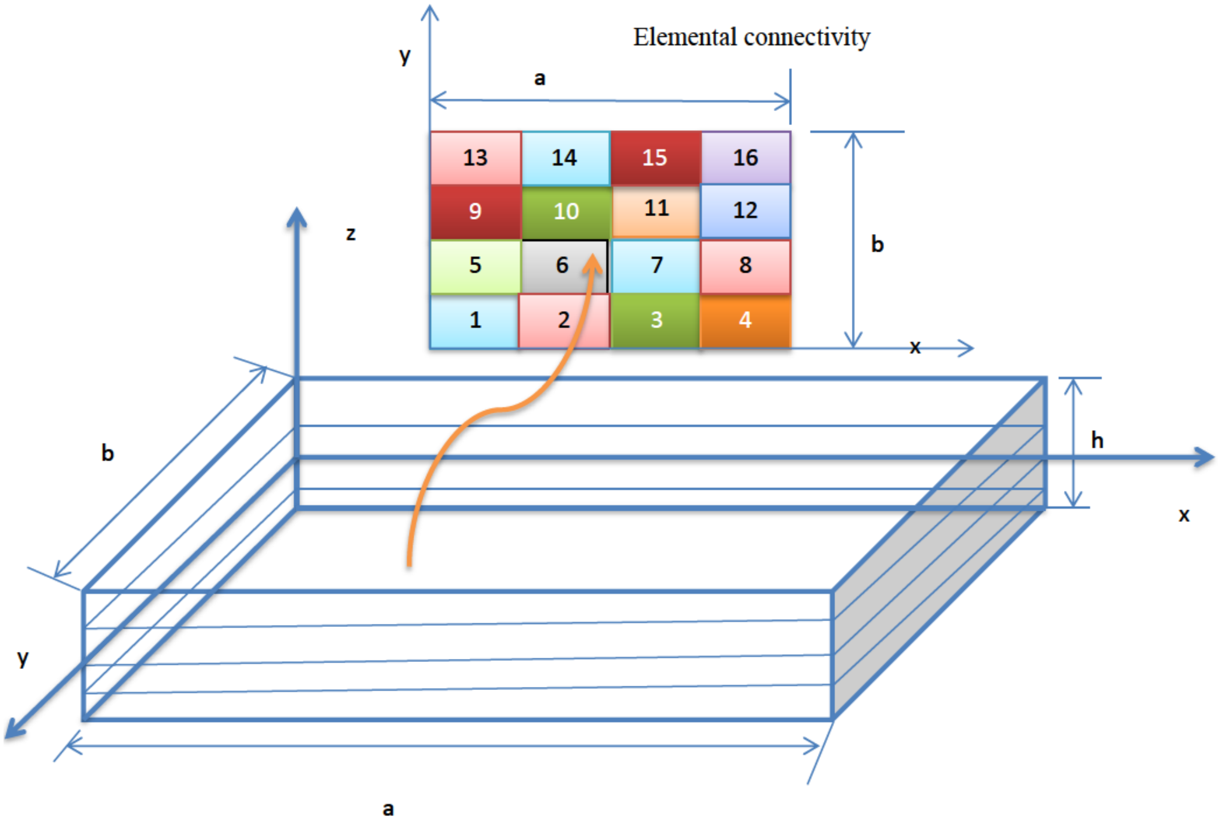

Figure 3: Laminated SWCNTRC-FG composite plate discretised into 4X4 nine noded isoperimetric elements.

$$V_{CNT} = 4\left(1 - \frac{2\,|z|}{h}\right) V\star - - - - - - - - - \text{FG-}\Delta$$

$$V^\star = \frac{W_{CNT}}{W_{CNT} + \left(\frac{\rho_{CNT}}{\rho_m}\right)(1 - W_{CNT})}$$

3 Basic HSDT

The laminated SWCNTRC plate is shown in Fig. 3. The linear bending formulation of laminated SWCNT-FG plate is derived. The displacement field of the higher order shear deformation Theory (HSDT) taken from [30]

3.1 Displacement field model

The displacement field for laminated SWCNTRC plate is given by [30],

$$\begin{aligned}\overline{u} &= u + z\psi_x - z^3\frac{4}{3h^2}\left(\frac{\partial w}{\partial x} + \psi_x\right) \\ &= u + f_1(z)\psi_x + f_2(z)\frac{\partial w}{\partial x}\end{aligned} \tag{12}$$

$$\begin{aligned}\overline{v} &= v + z\psi_y - z^3\frac{4}{3h^2}\left(\frac{\partial w}{\partial y} + \psi_y\right) \\ &= u + f_1(z)\psi_y + f_2(z)\frac{\partial w}{\partial y} \\ \overline{w} &= w\end{aligned}$$

Where $f_1(z) = C_1 z - C_2 z^3$, and $f_2(z) = -C_4 z^3; C_1 = 1,\ C_4 = C_2 = \frac{4}{3h^2}$;

It can be seen that the number of degrees of freedom (DOF) per node, by treating θ_x and $\theta_y$as separate DOFs, increases from 5 to 7 for HSDT model. However, the strain vector will be having only first order derivatives, and hence a C^0 continuous element would be sufficient for the finite element analysis by [30]

3.2 Strain displacement relation

By assuming small deformation, the linear strain vectors corresponding to displacement fields are,

$$\{\varepsilon\} = \{\varepsilon_1, \varepsilon_2, \varepsilon_3, \varepsilon_4, \varepsilon_5, \varepsilon_6\}^T \tag{13}$$

Where, ${\varepsilon_i}^0(i = 1, 2 \ldots 6)$ and ${k_i}^0(i = 1, 2 \ldots 6)$ are mid-plane strains and curvatures respectively, are given by [30]

$$\varepsilon_1 = \varepsilon_1^o + z(k_1^o + z^2 k_1^2), \tag{14}$$

$$\varepsilon_2 = \varepsilon_2^o + z(k_2^o + z^2 k_2^2),$$
$$\varepsilon_3 = 0, \quad \varepsilon_4 = \varepsilon_4^o + z^2 k_4^2,$$
$$\varepsilon_5 = \varepsilon_5^o + z^2 k_5^2, \quad \varepsilon_6 = \varepsilon_6^o + z(k_6^o + z^2 k_6^2)$$

Where,

$$\varepsilon_1^o = \frac{\partial u}{\partial x}, \quad k_1^o = \frac{\partial \psi_x}{\partial x}, \quad k_1^2 = -\frac{4}{3h^2}\left(\frac{\partial^2 w}{\partial x^2} + \frac{\partial \psi_x}{\partial x}\right);$$
$$\varepsilon_2^o = \frac{\partial u}{\partial y}, \quad k_2^o = \frac{\partial \psi_y}{\partial y}, \quad k_2^2 = -\frac{4}{3h^2}\left(\frac{\partial^2 w}{\partial y^2} + \frac{\partial \psi_y}{\partial y}\right)$$
$$\varepsilon_6^o = \frac{\partial u}{\partial x} + \frac{\partial v}{\partial y}, \quad k_6^o = \frac{\partial \psi_x}{\partial y} + \frac{\partial \psi_y}{\partial x},$$
$$k_6^2 = -\frac{4}{3h^2}\left(\frac{\partial \psi_x}{\partial y} + \frac{\partial \psi_y}{\partial x} + 2\frac{\partial^2 w}{\partial xy}\right)$$
$$\varepsilon_4^o = \psi_y + \frac{\partial w}{\partial y}, \quad k_4^2 = -\frac{4}{h^2}\left(\psi_y + \frac{\partial w}{\partial y}\right)$$
$$\varepsilon_5^o = \psi_x + \frac{\partial w}{\partial x}, \quad k_5^2 = -\frac{4}{h^2}\left(\psi_x + \frac{\partial w}{\partial x}\right)$$

Here, the mid-plane strain vector can be written as

$$\{\overline{\varepsilon}\} = \left(\varepsilon_1^0\ \varepsilon_2^0\ \varepsilon_6^0\ k_1^0\ k_2^0\ k_6^0\ k_1^2\ k_2^2\ k_6^2\ \varepsilon_4^0\ \varepsilon_5^0\ k_4^2\ k_5^2\right), \quad (15)$$

The mid-plane displacement vector for the modified C_0 continuous model can be written as

$$q = \{u\ v\ w\ \theta_y\, \theta_x\ \ \psi_y\, \psi_x\}^T \quad (16)$$

3.3 Constitutive equation (stress-strain relation)

Stress is related to strain by following relation

$$\{\sigma\} = \left[\overline{Q}\right]\{\varepsilon\} \quad (17)$$

The stress vector by considering $\sigma_z = 0$ and $\varepsilon_z = 0$ can be written as:

$$\begin{Bmatrix} \sigma_x \\ \sigma_y \\ \tau_{xy} \\ \tau_{y_z} \\ \tau_{xz} \end{Bmatrix} = \begin{Bmatrix} \sigma_1 \\ \sigma_2 \\ \tau_6 \\ \tau_4 \\ \tau_5 \end{Bmatrix} \quad (18)$$
$$= \begin{bmatrix} \overline{Q}_{11} & \overline{Q}_{12} & \overline{Q}_{16} & 0 & 0 \\ \overline{Q}_{12} & \overline{Q}_{22} & \overline{Q}_{26} & 0 & 0 \\ \overline{Q}_{16} & \overline{Q}_{26} & \overline{Q}_{66} & 0 & 0 \\ 0 & 0 & 0 & \overline{Q}_{44} & \overline{Q}_{45} \\ 0 & 0 & 0 & \overline{Q}_{45} & \overline{Q}_{55} \end{bmatrix} \begin{Bmatrix} \varepsilon_x \\ \varepsilon_y \\ \gamma_{xy} \\ \gamma_{yz} \\ \gamma_{xz} \end{Bmatrix};$$

$$[\overline{Q}] = \begin{bmatrix} \overline{Q}_{11} & \overline{Q}_{12} & \overline{Q}_{16} & 0 & 0 \\ \overline{Q}_{12} & \overline{Q}_{22} & \overline{Q}_{26} & 0 & 0 \\ \overline{Q}_{16} & \overline{Q}_{26} & \overline{Q}_{66} & 0 & 0 \\ 0 & 0 & 0 & \overline{Q}_{44} & \overline{Q}_{45} \\ 0 & 0 & 0 & \overline{Q}_{45} & \overline{Q}_{55} \end{bmatrix}$$ is the elasticity matrix.

Where,

$$\overline{Q}_{11} = Q_{11}\cos^4\theta_k + Q_{22}\sin^4\theta_k + 2\left(Q_{12} + 2Q_{66}\right)\sin^2\theta_k\cos^2\theta_k,$$
$$\overline{Q}_{12} = (Q_{11} + Q_{22} - 4Q_{66})\sin^2\theta_k\cos^2\theta + Q_{12}\left(\cos^4\theta_k + \sin^4\theta_k\right),$$
$$\overline{Q}_{22} = Q_{22}\cos^4\theta_k + Q_{11}\sin^4\theta_k + 2\left(Q_{12} + 2Q_{66}\right)\sin^2\theta_k\cos^2\theta_k,$$
$$\overline{Q}_{16} = \left(Q_{11} - Q_{12} - 2Q_{66}\right)\sin\theta_k\cos^3\theta_k + \left(Q_{12} - Q_{22} + 2Q_{66}\right)\sin^3\theta_k\cos\theta_k,$$
$$\overline{Q}_{26} = (Q_{11} - Q_{12} - 2Q_{66})\sin^3\theta_k\cos\theta_k + \left(Q_{12} - Q_{22} + 2Q_{66}\right)\sin\theta_k\cos^3\theta_k,$$
$$\overline{Q}_{44} = Q_{44}\cos^2\theta_k + Q_{55}\sin^2\theta_k,$$
$$\overline{Q}_{45} = \left(Q_{55} - Q_{44}\right)\sin\theta_k\cos\theta_k = \overline{Q}_{54},$$
$$\overline{Q}_{55} = Q_{55}\cos^2\theta_k + Q_{44}\sin^2\theta,$$
$$\overline{Q}_{66} = \left(Q_{11} + Q_{22} - 2Q_{12} - 2Q_{66}\right)\sin^2\theta_k\cos^2\theta_k + Q_{66}\left(\cos^4\theta_k + \sin^4\theta_k\right),$$

Material stiffness coefficients $\left[Q_{ij}\right]$ are given by

$$Q_{11} = \frac{E_{11}}{(1 - \nu_{12}\nu_{21})}, \quad Q_{12} = \frac{\nu_{12}E_{22}}{(1 - \nu_{12}\nu_{21})}, \quad (19)$$
$$Q_{21} = \frac{\nu_{21}E_{11}}{(1 - \nu_{12}\nu_{21})}, \quad Q_{22} = \frac{E_{22}}{(1 - \nu_{12}\nu_{21})},$$
$$Q_{55} = Q_{66} = G_{12} \text{ and } Q_{44} = G_{13}$$

3.4 Finite element modelling

The finite element method (FEM) is a numerical technique being used for finding an approximate solution to a wide variety of engineering problems through bending Approach. In the present paper nine nodded isoperimetric elements with seven degree of freedom per node is employed for finite element of SWCNTRC-FG plate modelling.

$$q = \sum_{i=1}^{NN} N_i q_i; \quad x = \sum_{i=1}^{NN} N_i x_i; \quad y = \sum_{i=1}^{NN} N_i y_i \quad (20)$$

Where, N_i and q_i are the interpolation function and vector of unknown displacements for the i^{th} node, respectively, NN is the number of nodes per element and x_i and y_i are Cartesian coordinate of the i^{th} node. The strain are related to displacement by strain-displacement matrix $[B_i]$

$$\{\overline{\varepsilon_l}\}_{13\times1} = [B_i]_{13\times7}\{N_i\}_{7\times1} \quad (21)$$

$$
\{\overline{\varepsilon_l}\} = \begin{Bmatrix} \varepsilon_1^0 \\ \varepsilon_2^0 \\ \varepsilon_6^0 \\ k_1^0 \\ k_2^0 \\ k_6^0 \\ k_1^2 \\ k_2^2 \\ k_6^2 \\ \varepsilon_4^0 \\ \varepsilon_5^0 \\ k_4^2 \\ k_5^2 \end{Bmatrix} = \begin{bmatrix} \partial/\partial x & 0 & 0 & 0 & 0 & 0 & 0 \\ 0 & \partial/\partial y & 0 & 0 & 0 & 0 & 0 \\ \partial/\partial y & \partial/\partial x & 0 & 0 & 0 & 0 & 0 \\ 0 & 0 & 0 & 0 & 0 & 0 & C1\partial/\partial x \\ 0 & 0 & 0 & 0 & 0 & C1\partial/\partial y & 0 \\ 0 & 0 & 0 & 0 & 0 & C1\partial/\partial x & C1\partial/\partial y \\ 0 & 0 & 0 & 0 & -C4\partial/\partial x & 0 & -C2\partial/\partial x \\ 0 & 0 & 0 & -C4\partial/\partial y & 0 & -C2\partial/\partial y & 0 \\ 0 & 0 & 0 & -C4\partial/\partial x & -C4\partial/\partial y & -C2\partial/\partial x & -C2\partial/\partial y \\ 0 & 0 & C1\partial/\partial y & 0 & 0 & C1 & 0 \\ 0 & 0 & C1\partial/\partial x & 0 & 0 & 0 & C1 \\ 0 & 0 & 0 & -3C4 & 0 & -3C2 & 0 \\ 0 & 0 & 0 & 0 & -3C4 & 0 & -3C2 \end{bmatrix} \begin{Bmatrix} u \\ v \\ w \\ \theta_y \\ \theta_x \\ \psi_y \\ \psi_x \end{Bmatrix},
$$

The elemental stiffness matrices $\left[k^e\right]$ can be expressed as

$$
\left[k^e\right] = \int_{A^e} \{B\}^T [D] \{B\} \, dA \tag{22}
$$

Where, [D] is a material property matrix, defined as:

$$
D = \sum_{k=1}^{NL} \int_{z_{k-1}}^{z_k} [T]^T \left[\overline{Q}_{ij}\right] [T] \, dz = \begin{bmatrix} [A_1][B][E]00 \\ [B][C_1][F_1]00 \\ [E][F_1][H]00 \\ 000[A_2][C_2] \\ 000[C_2][F_2] \end{bmatrix} \tag{23}
$$

With,

$$
\left(A_{1_{ij}}, B_{ij}, \quad C_{1_{ij}}, \quad E_{ij}, \quad F_{1_{ij}}, \quad H_{ij}\right) = \sum_{k=1}^{NL} \int_{z_{k-1}}^{z_k} \overline{Q}_{ij}^{(k)} \left(1, \quad z, \quad z^2, \quad z^3, \quad z^4, \quad z^6\right) dz, \tag{24}
$$

For i,j=1,2,6,

$$
\left(A_{2_{ij}}, \quad C_{2_{ij}}, \quad F_{2_{ij}},\right) = \sum_{k=1}^{NL} \int_{z_{k-1}}^{z_k} \overline{Q}_{ij}^{(k)} \left(1 \quad z \quad z^4,\right) dz \tag{25}
$$

The elemental stiffness matrix in natural coordinate system (ξ, η) can be expressed as

$$
\left[k^e\right] = \int_{-1}^{1} \int_{-1}^{1} [B]^T [D] [B] \det[J] \, d\xi d\eta \tag{26}
$$

Where, the Jacobin [J] is

$$
[J] = \begin{bmatrix} \frac{dx}{d\xi} & \frac{dy}{d\xi} \\ \frac{dx}{d\eta} & \frac{dy}{d\eta} \end{bmatrix}
$$

3.5 Potential energy of the SWCNTRC plate

The total potential energy of SWCNTRC plate is sum of potential energy due to internal strain energy U_1 and potential energy due to external applied loading U_2 and given by

$$
U^e = \sum_{e=1}^{NE} U_1^e - \sum_{e=1}^{NE} U_2^e \tag{27}
$$

The internal potential energy in the form of strain energy is given by

$$U_1^e = \frac{1}{2}\int_{A^e} [\bar{\varepsilon}]^T \{[D]\} [\bar{\varepsilon}]\, dA \tag{28}$$

The mid-plain strain $\{\bar{\varepsilon}\}$ can be written in terms of displacement as

$$\{\bar{\varepsilon}\}_{13\times1} = [B_i]_{13\times7}\{N_i\}_{7\times1} \tag{29}$$

Using Eq. (28) and (29) can be obtained

$$U_1^e = \frac{1}{2}\int_{A^e} \{q\}^T [B_i]^T [D] [B_i] \{q\} [\bar{\varepsilon}]\, dA \tag{30}$$

Substituting Eq. (20) in Eq. (30) we obtained

$$U_1^e = \frac{1}{2}\int_{A^e} \left\{ \left(\sum_{i=1}^{NN} \{q_i\}^T [B_i] N_i \right) [D] \left(\sum_{i=1}^{NN} \{q_i\} [B_i] N_i \right) \right\} dA \tag{31}$$

Eq. (31) simplified by

$$U_1^e = \frac{1}{2}\int_{A^e} \{q\}^T [B] [D] [B] \{q\}\, dA \tag{32}$$

Where, q is a generated displacement vector for the SWCNTRC plate.

The elemental potential energy due to external applied loading is given by

$$U_2^e = \int_A \{q\}^T \boxed{F}\, dA \tag{33}$$

Where, $\boxed{F}$ is load vector corresponds to each DOF. For the present case uniform transverse loading $\boxed{F}$ can be written as

$$\boxed{F} = \left\{ 00P0000 \right\}^T \tag{34}$$

Substituting for $\{q\}$ form Eq. (20) in Eq. (33) we obtained

$$U_2^e = \int_{A^e} \left(\sum_{i=1}^{NN} \{q_i\}^T N_i \right) \left\{ \bar{F}_i^{\,(e)} \right\}^T dA \tag{35}$$

$$U_2^e = \left\{ q^{(e)} \right\}^T \left\{ F^{(e)} \right\}$$

Where,

$$\left\{ F^{(e)} \right\} = \int_{A^e} \{N\}^e \{\bar{F}\}^e dA$$

The equilibrium Equation governing the present problem for the SWCNTRC plate can obtain by minimizing potential energy with respect to displacement. Substituting Eq. (32) and Eq. (35) into Eq. (27) and minimizing with respect to $\{q\}$, we obtained

$$\{F_i\} = [K_{ij}] \{q_i\} \tag{36}$$

Where, $\{F_i\} = -\sum_{e=1}^{NE} \{F\}^e$ is global force vector, $[K_{ji}] = \sum_{e=1}^{NE} \left[K_{ij}^e\right]$ is global stiffness matrix, $\{q_i\} = \sum_{e=1}^{NE} \{q\}^e$ is global displacement vector.

4 Results and discussion

The liner bending finite element method code in MATLAB13.0 has been developed following analysis stapes discussed previous section. In order to demonstrate accuracy and applicability of present formulation is validated with published literature. Laminated SWCNTRC plate has been discretised into 4X4 by using nine nodes isoperimetric Lagrange quadratic element as shown in Fig. 3. Tables 1 and 2 shows the Non-dimensional displacement for different boundary condition with varying aspect ratio (a/h) and volume fraction. It is good agreement of present results. An nine noded quadratic element with 7 degrees of freedom per node for the present HSDT. Linear node has been proposed and describing the laminated SWCNTRC as C_o continuity. The Property of SWCNT (20, 20) is taken from [28], $E_{11}^{CNT} = 158.244$ GPa, $E_{22}^{CNT} = 17$ GPa, $G_{12}^{CNT} = G_{23}^{CNT} = 2.79$ GPa, $\nu_{12}^{CNT} = \nu_{21}^{CNT} = 0.32$, $\nu_{23}^{CNT} = 0.78$ and Matrix material-EPON-862: $E_m = 3.07$ GPa, $\nu_m = 0.3$, a = 5 mm and b = 10 mm. The bending analysis of laminated SWCNTRC plates under uniformly transversely load is considered. Over all property of laminated SWCNTRC plate is calculated from Eq. (10).

Following boundary condition is taken for a plate.

All edge simply supported edges (SSSS)

$u = v = w = \psi_y = \theta_y = 0$ at x=0 and a.

$u = v = w = \psi_x = \theta_x = 0$ at y=0 and b.

All edge clamped (CCCC)

$u = v = w = \psi_x = \psi_y = \theta_x = \theta_y = 0$ at x=0, a and y=0, b

Figure 4 present non-dimensional central deflections (W_0) versus width-to-thickness ratio for different lamination scheme with UD distribution of plate subjected to uniform transverse loading (q_0). The results clearly show that the non-dimensional central deflection decrease with an increase the width-to-thickness ratio. All lamination schemes have significant results of the a/h ratio up to 20 and rest of the value is constant.

Table 1: Non-dimensional displacement based on volume fraction of SWCNT (V_{CNT}) of validated results from Lei *et al.* [7].

		SSSS		CCCC		CFCF		CFFF	
V_{CNT}		Lei *et al.* [7]	Present	Lei *et al.* [7]	Present	Lei *et al.* [7]	Present	Lei *et al.* [7]	Present
0.11	UD	7.3234	7.3200	3.8306	3.8306	5.4371	5.4370	28.6211	28.6210
	FG-V	7.3165	7.3095	3.8332	3.8032	5.4327	5.4320	28.6908	28.6808
	FG-O	7.3982	7.3985	3.8440	3.8440	5.4488	5.4488	28.77703	28.7875
	FG-X	7.2150	7.2087	3.7889	3.7889	5.4135	5.4030	28.335	28.3540
0.14	UD	6.3455	6.3454	3.5060	3.5142	5.0539	5.0654	24.8896	24.8972
	FG-V	6.3264	6.3250	3.4965	3.4965	5.0505	5.0505	24.8831	24.8831
	FG-O	6.3955	6.3950	3.5153	3.4853	5.0840	5.0850	24.9450	24.9442
	FG-X	6.2405	6.2015	3.4590	3.4590	5.0352	5.0354	24.6011	24.6011
0.17	UD	4.7024	4.5871	2.4289	2.4289	3.4210	3.4224	18.3666	18.3666
	FG-V	4.678	4.564	2.4221	2.4220	3.4181	3.4178	18.3356	18.3587
	FG-O	4.7314	4.7315	2.4365	2.4365	3.4544	3.4588	18.3871	18.3871
	FG-X	4.6117	4.6117	2.3931	2.3931	3.4054	3.4054	18.1007	18.1007

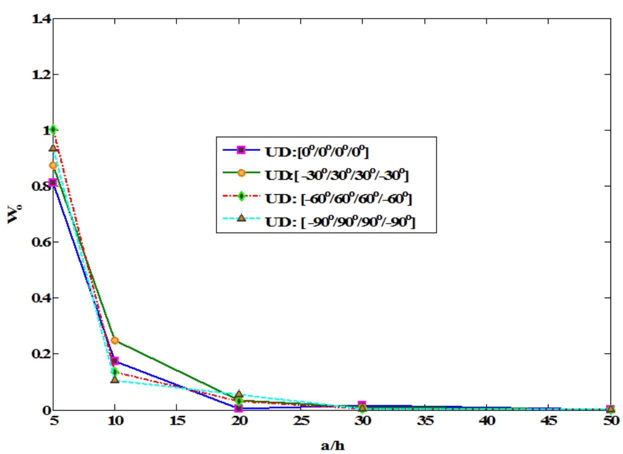

Figure 4: The non-dimensional deflection W_o for angle–ply [-θ/θ/θ/-θ] UD plate with different lamination scheme

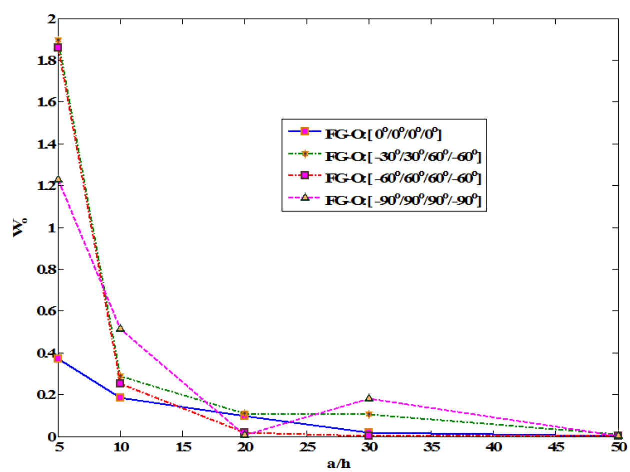

Figure 5: The non-dimensional deflection W_o for angle–ply [-θ/θ/θ/-θ] FG-O plate with different lamination scheme

Figure 5 shows non-dimensional central deflections (W_0) versus width-to-thickness ratio for different lamination scheme with FG-O distribution of plate subjected to uniform transverse loading (q_0). The results clearly show that the non-dimensional central deflection decrease with an increase the width-to-thickness ratio. All lamination schemes have significant results of the a/h ratio up to 20 and the rest of the value is constant.

Figure 6 present non- dimensional central deflections (W_0) versus width-to-thickness ratio for different lamination scheme with FG-V distribution of plate subjected to uniform transverse loading (q_0). The results clearly show that the non-dimensional central deflection decrease with an increase the width-to-thickness ratio. Because of a/h > 20 plate is thin and plate a/h < 20 plate is thick. However, lamination scheme [0/0/0/0] plate is more stiffness as compare to other lamination scheme.

Figure 7 depicts non- dimensional central deflections (W_0) versus width-to-thickness ratio for different lamination scheme with FG-A distribution of plate subjected to uniform transverse loading (q_0). The results clearly show that the non-dimensional central deflection decrease with an increase the width-to-thickness ratio. The suddenly change deflection to increase the a/h ratio up to 20. So that significant value of plate a/h is 20 because plates become thick.

Figure 8 shows the non-dimensional central normal stresses σ_{xx} distributed along the non-dimensional thickness (z/h) of various lamination scheme of SWCNTRC-UD plate with four edge simply supported subjected to uni-

Table 2: Non-dimensional displacement based on aspect ratio (a/h) of validated results from Lei *et al.* [7]

a/h		SSSS		CCCC		CFCF		CFFF	
		Lei *et al.* [7]	Present	Lei *et al.* [7]	Present	Lei *et al.* [7]	Present	Lei *et al.* [7]	Present
10	UD	7.3234	7.3234	3.8306	3.8006	5.4371	5.4370	28.6211	28.621
	FG-V	7.3165	7.3254	3.8332	3.8332	5.4327	5.4327	28.6908	28.690
	FG-O	7.3982	7.3980	3.8440	3.8570	5.4488	5.4489	28.7703	28.7703
	FG-X	7.2150	7.2150	3.78889	3.7898	5.4135	5.4136	28.3350	28.3350
20	UD	4.8928	4.8928	1.6495	1.5350	1.9832	1.9000	18.1915	18.1920
	FG-V	4.8962	4.8960	1.6581	1.6542	1.9850	1.8790	18.3139	18.3254
	FG-O	4.9657	4.9658	1.6659	1.5866	1.9895	1.9894	18.3932	18.4065
	FG-X	4.8100	4.8122	1.6255	1.6055	1.9653	1.9653	17.9591	17.9590
50	UD	4.1634	4.1634	0.9596	0.9596	1.0156	1.0154	15.2643	15.2645
	FG-V	4.1702	4.1875	0.9687	0.9687	1.0224	1.2265	15.4013	15.4016
	FG-O	4.2359	4.2395	0.9748	0.9747	1.0269	1.0296	15.4807	15.4807
	FG-X	4.0887	4.0897	0.9431	0.9431	1.0026	1.0026	15.0470	15.0458

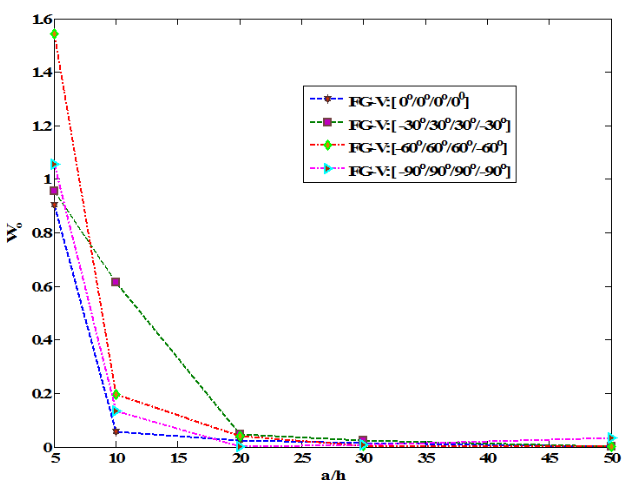

Figure 6: The non-dimensional deflection W_o for angle–ply [-θ/θ/θ/-θ] FG-V, SWCNT-FG plate with different lamination scheme

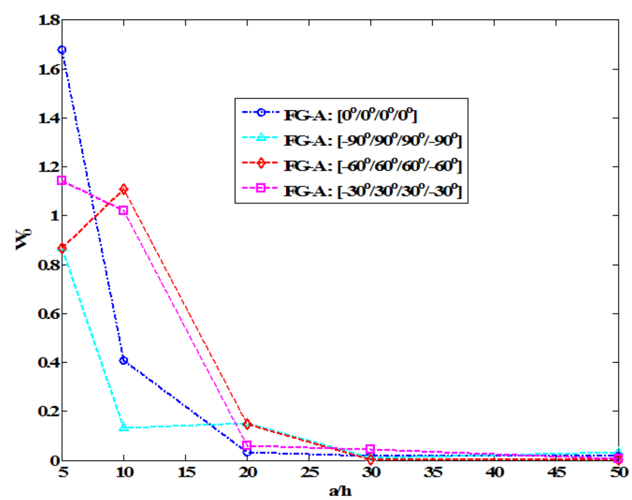

Figure 7: The non-dimensional deflection W_o for angle–ply [-θ/θ/θ/-θ] FG-A plate with different lamination scheme

form transverse load q_0 with volume fraction V_{CNT} = 0.11 and width-to-thickness ratio a/h = 20. It can be found that the central normal stress distribution in different lamination scheme of plates is anti-symmetric about the mid-plane due to the symmetric reinforcement with respect to the mid-plane. However, lamination scheme [0/0/0/0] plate has more stiffness.

Figure 9 presents the non-dimensional normal stresses σ_{yy} distributed along the non-dimensional thickness (z/h) of various lamination scheme of SWCNTRC-UD plate with four edges simply supported subjected to uniform transverse load q_0 with volume fraction V_{CNT} = 0.11 and width-to-thickness ratio a/h = 20. It can be found that the central normal stress distribution in different lamination scheme of plates is anti-symmetric about the mid-plane due to the symmetric reinforcement with respect to the mid-plane. However, lamination scheme [−60/60/60/−60] plate have more stiffness.

Figure 10 shows the non-dimensional normal stresses σ_{xx} distributed along the non-dimensional thickness (z/h) of various lamination scheme of SWCNTRC-FG-V plate with four edges simply supported subjected to uniform transverse load q_0 with volume fraction V_{CNT} = 0.11 and width-to-thickness ratio a/h = 20. It can be found that the central normal stress distribution in different lamination scheme of bottom surface of the plates is weak as compare to top surface. Because of SWCNT is in rich at top surface of

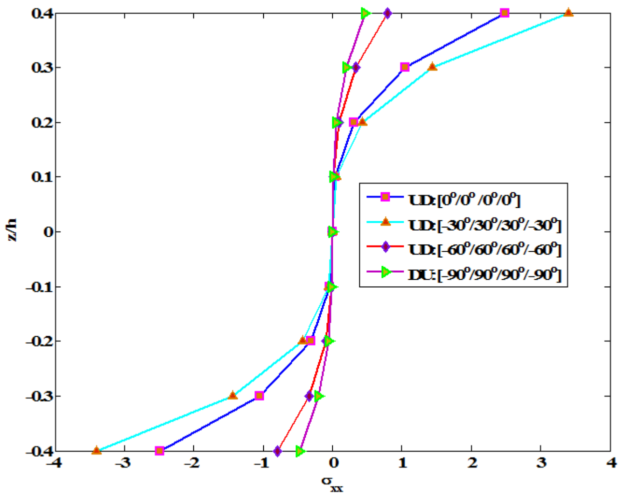

Figure 8: The non-dimensional stress σ_{xx} for angle–ply [-θ/θ/θ/-θ] UD plate with different lamination scheme

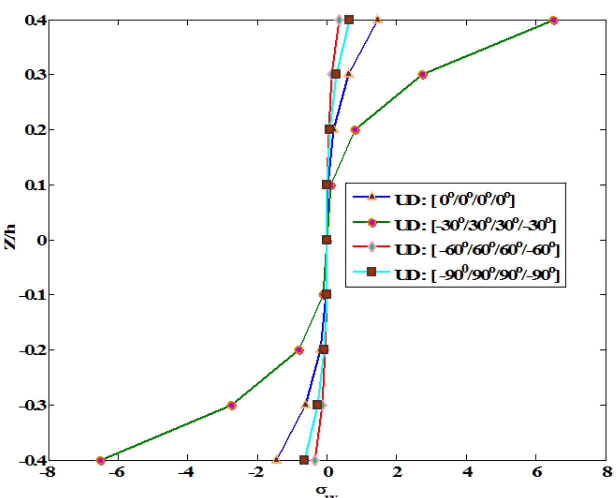

Figure 9: The non-dimensional stress σ_{yy} for angle–ply [-θ/θ/θ/-θ] UD plate with different lamination scheme

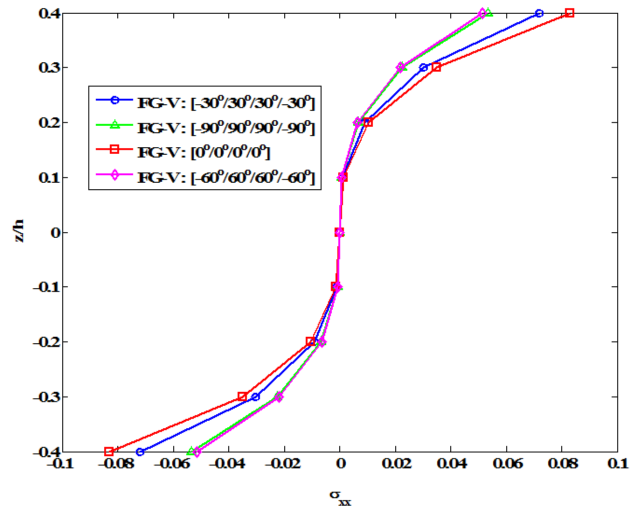

Figure 10: The non-dimensional stress σ_{xx} for angle–ply [-θ/θ/θ/-θ] FG-V SWCNT-FG plate with different lamination scheme

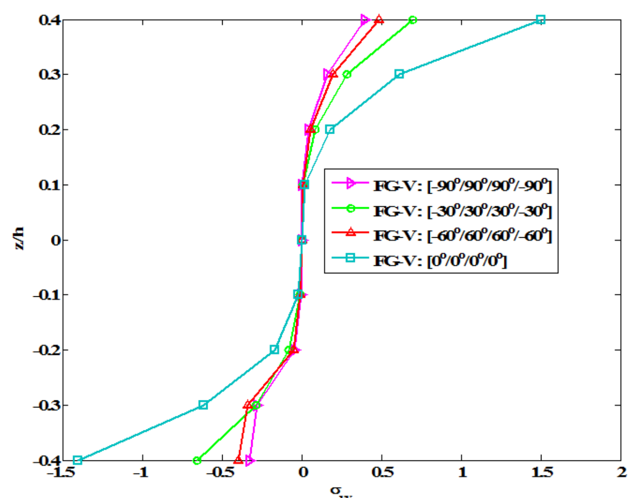

Figure 11: The non-dimensional stress σ_{yy} for angle–ply [-θ/θ/θ/-θ] FG-V SWCNT-FG plate with different lamination scheme

plate. However, lamination scheme [−60/60/60/−60] plate have more stiffness.

Figure 11 shows the non-dimensional normal stresses σ_{yy}distributed along the non-dimensional thickness (z/h) of various lamination scheme of SWCNTRC-FG-V plate with four edges simply supported subjected to uniform transverse load q_0 with volume fraction V_{CNT} = 0.11 and width-to-thickness ratio a/h = 20. It can be found that the central normal stress distribution in different lamination scheme of the bottom surface of the plates is weak as compare to top surface. Because of SWCNT is in rich at the top surface of the plate.

Figure 12 presents the non-dimensional normal stresses σ_{xx} distributed along the non-dimensional thickness (z/h) of various lamination scheme of SWCNTRC-FG-X plate with four edges simply supported subjected to uniform transverse load q_0 with volume fraction V_{CNT} = 0.11 and width-to-thickness ratio a/h = 20. It can be found that the normal stress distribution in different lamination scheme of top and bottom surface of the plates. The SWCNT is in rich at top and bottom surface of the plate.

Figure 13 shows the non-dimensional normal stresses σ_{yy}distributed along the non-dimensional thickness (z/h) of various lamination scheme of SWCNTRC-FG-X plate with four edges simply supported subjected to uniform transverse load q_0 with volume fraction V_{CNT} = 0.11 and width-to-thickness ratio a/h = 20. It can be found that the central normal stress distribution in different lamination scheme of top and bottom surface of the

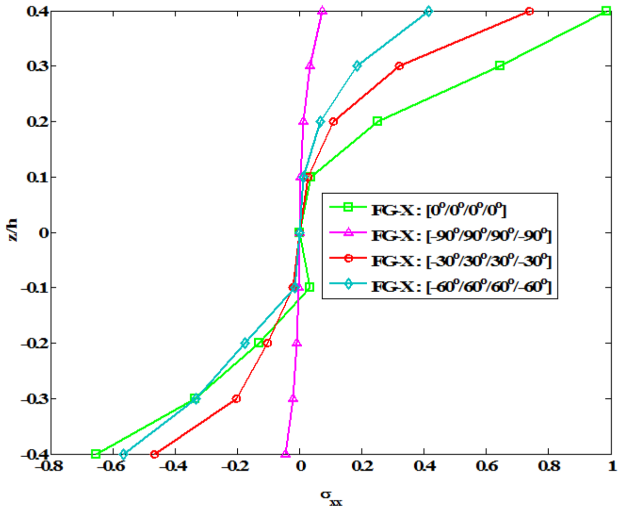

Figure 12: The non-dimensional stress σ_{xx} for angle–ply [-θ/θ/θ/-θ] FG-X SWCNT-FG plate with different lamination scheme

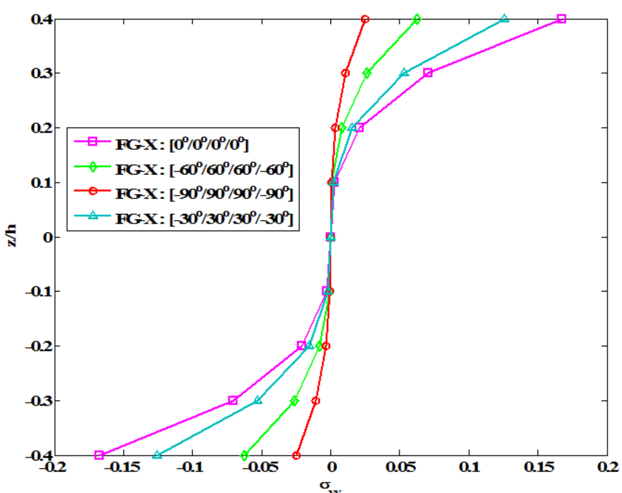

Figure 13: The non-dimensional stress σ_{yy} for angle–ply [-θ/θ/θ/-θ] FG-X SWCNT-FG plate with different lamination scheme

plates. The SWCNT is in rich at the top and bottom surface of the plate. Also, it can be seen a large variation of stresses along the thickness direction for lamination scheme [−90/90/90/−90]. Because of SWCNT is transverse to the reference plane.

5 Conclusion

In this study, the bending behaviour of the laminated SWCNT reinforced composite plate of five different grading (UD, FG-X, FG-O,FG-A and FG-V) under uniform transverse loading have been examined using the HSDT kinematic model. The laminated SWCNTRC-FG plate is embedded of perfect bonded Epon-862 matrix layer. The each layer SWCNT is assumed to be functionally graded in the thickness direction. The structure is graded functionally through the thickness based on the volume fractions of the CNT, and the effective properties are evaluated through the micromechanical model using the Mori-Tanaka. The desired governing equation for the bending analysis is obtained using minimum potential energy principle and discretized through the suitable isoperimetric finite element steps. The model has also been validated by comparing the responses to results available in the literature. The applicability of the present higher-order model has been highlighted by computing the responses for the different geometrical and material parameters.

Following points are concluded

1. The close agreement between the results obtained by the present approach and those appearing in the published literature establishes the correctness of the formulation.
2. Central non dimensional deflection is minimum for lamination scheme [0/0/0/0] plate, so that more stiffness of the plate.
3. The significant deflection of laminated plate is width-to-thickness ratio up to 20.
4. Laminated SWCNT-FG-X plates are stiffer than the other plate, because SWCNT-Rich at the top and bottom surface of the plate.
5. The maximum stress is present in the lamination scheme [0/0/0/0] while minimum stress is presented in lamination scheme [−90/90/90/−90].

References

[1] Salami Jedari S., Extended high order sandwich panel theory for bending analysis of sandwich beams with carbon nanotube reinforced face sheets, Physica-E 2016, 76, 187–197

[2] Wuite J., Adali S., Deflection and stress behavior of nano composite reinforced beam using a multi-scale analysis, Composite Structures, 2005, 71, 388-396.

[3] Vodenitcharova T, Zhang L.C., Bending and local buckling of a nanocomposite beam reinforced by a single walled carbon nanotube. Int J Solids and Struct, 2006, 43, 3006–3024.

[4] Malekzadeh P., Shojaee M.., Buckling analysis of quadrilateral laminated plates with carbon nanotubes reinforced composite layers, Thin-Walled Structures, 2013, 71, 108–118

[5] Wattanasakulpong Nuttawit, Chaikittiratana Arisara, Exact solution for static and dynamic analysis of carbon nanotube–reinforced composite plate with Pasternak elastic foundation, Applied Mathematical Modeling, 2015, 39, 5459–5472

[6] Lei Z.X., liew K.M, Yu J.L., Large deflection analysis of functionally graded carbon nanotube reinforced composite plates by the element free kp-ritz method, Computational Methods Applied

Mechanics And Engineering, 2013, 256, 189-199.
[7] Lei Z.X., Zhang L.W., Liew K.M., Analysis of laminated CNT reinforced functionally graded plates using the element-free kp-ritz method, Composites Part-B, 2016, 84, 211-221.
[8] Zhu P., Lei Z.X., liew K.M., Static and dynamic analyses of carbon nanotube-reinforced composite plates using finite element method with first order shear deformation plate theory ,Composite Structures, 2012, 94, 1450-1460.
[9] Mudhu S., Subba Rao V.V., Effect of carbon nanotube reinforcement in polymer composite plates under static loading ,International Journal Of Chemical, Molecular, Nuclear, Materials And Metallurgical Engineering, 2014, 8(3).
[10] Mohammadpour Ehsan, Awing Mokhtar, Kakooei Saeid, Akil Hazizan Md, Modeling the tensile stress-strain response of carbon nanotube /polypropylene, nano composite using nonlinear representative volume element, Materials and Design, 2014, 58, 36-42.
[11] Seidel Gary D., Lagoudas dimitris., Micromechanical analysis of the effective elastic property of carbon nanotube reinforced composites, Mechanics Of Materials, 2006, 38, 884-907
[12] Hu Hurang, onyebueke Landon, Abatan Ayo, Characterizing and modeling mechanical properties of nanocomposites review and evaluation, Journal Of Minerals And Materials Characterization And Engineering, 2010, 9(4), 275-319.
[13] Shi Dong-Li, Feng Xi-Qiao,Yonggang Huang Y., Hwang Keh-Chih, Gao Huajian., The effect of nanotube waviness and agglomeration on the elastic property of carbon nanotube reinforced composites, Transactions of the ASME, july 2004, 2(16), 250
[14] Ghugal Yuwaraj M., Sayyad Atteshamuddin S., Stress analysis of thick laminated plates using trigonometric shear deformation theory, International Journal Of Applied Mechanics, 2013, 5(1), 23
[15] Sayyad S., Ghugal Y. M., Effect of stress concentration on laminated plates, Journal of Mechanics, 2012, 29(02), 241-252.
[16] Mareishi Soraya, Kalhori Hamed, Rafiee Mohammad, and Hosseini Seyedeh Marzieh, Nonlinear forced vibration response of smart two-phase nano-composite beams to external harmonic excitations, Curved and Layer. Struct., 2015, 2, 150–161
[17] Kundalwal S. I. , Meguid S. A., Effect of carbon nanotube waviness on active damping of laminated hybrid composite shells, Acta Mech, 2015, 226, 2035–2052.
[18] Pouresmaeeli S., Fazelzadeh S. A., Frequency analysis of doubly curved functionally graded carbon nanotube-reinforced composite panels, Acta Mech 2016, 227, 2765–2794
[19] Guz A. N., Rushchitsky J. J., Analysis of structurally complex Nano-composites (review), International Applied Mechanics, 2011, 47(4), 3–75.
[20] Pantano A., Cappello F., Numerical model for composite material with polymer matrix reinforced by carbon nanotubes, Meccanica, 2008, 43, 263–270.
[21] Wan H., Delale F., A structural mechanics approach for predicting the mechanical properties of carbon nanotubes, Meccanica, 2010, 45, 43–51.
[22] Cestari Clara Bertolini., Invernizzi Stefano, Marzi Tanja., Tulliani Jean-Marc., The reinforcement of ancient timber-joints with carbon nano-composites, Meccanica, 2013, 48, 1925–1935
[23] Kiani Keivan., Free vibrations of elastically embedded stocky single-walled carbon nanotubes acted upon by a longitudinally varying magnetic field, Meccanica, 2015, 50, 3041–3067
[24] Mirzaei M., Kiani Y., Thermal buckling of temperature dependent FG-CNT reinforced composite plates, Meccanica, 2016, 51, 2185–2201.
[25] Canadija Marko., Brcic Marino., Brnic Josip., Elastic properties of nanocomposite materials: influence of carbon nanotube imperfections and interface bonding, Meccanica, DOI 10.1007/s11012-016-0516-x.
[26] Kamarian S., Pourasghar A., Yas M. H., Eshelby-Mori-Tanaka approach for vibrational behavior of functionally graded carbon nanotube-reinforced plate resting on elastic foundation, Journal of Mechanical Science and Technology, 2013, 27 (11), 3395-3401.
[27] Shams Sh., Soltani B., Buckling of Laminated Carbon Nanotube-Reinforced Composite Plates on Elastic Foundations Using a Meshfree Method, Arab J Sci Eng, 2016, 41, 1981–1993.
[28] Han Y., Elliott J., Molecular dynamics simulations of the elastic properties of polymer/carbon Nanotube composites, Comput. Mater. Sci., 2007, 39, 315–323.
[29] Zhang L.W., Lei ZX, Liew KM, Yu J.L. Static and dynamic of carbon nanotube reinforced functionally graded cylindrical panels, Composite Structure, 2014, 111, 205-212.
[30] Reddy J.N., A simple higher order theory for laminated composite plates. ASME J Appl Mech, 1984, 51, 745–152